

STEELS FOR GENERAL ENGINEERING PURPOSES

UDC 539.377:669.15-194:539.25:539.42

EFFECT OF TEMPERING ON THE MICROSTRUCTURE AND MECHANICAL PROPERTIES OF HEAT-RESISTANT STEEL 10Kh9K3B2MFBR ALLOYED WITH Ta AND B

E. S. Tkachev,^{1,2} S. I. Borisov,^{1,2} Yu. I. Borisova,^{1,2} and R. O. Kaibyshev^{1,2}Translated from *Metallovedenie i Termicheskaya Obrabotka Metallov*, No. 3, pp. 10 – 19, March, 2024.*Original article submitted November 28, 2023.*

The effect of air quenching and subsequent tempering on the structure, mechanical properties and fracture mechanism of steel 10Kh9K3B2MFBR alloyed with tantalum and boron is studied. Transmission electron microscopy is used to show that after the air quenching, the steel acquires a structure of lath martensite with nanosize particles of (Nb, Ta)(C, N) carbonitride and cementite. Residual film-like austenite morphology is located over the boundaries of laths and blocks. The steel in this state is characterized by a high strength ($\sigma_{0.2} = 1020$ MPa) and an impact toughness of $24 \text{ J} \cdot \text{cm}^2$. During the low-temperature tempering, dispersion hardening and decomposition of retained austenite with precipitation of cementite chains along the lath boundaries lead to embrittlement. Increase of the tempering temperature in the range of $500 - 750^\circ\text{C}$ is accompanied by a monotonic decrease in the strength characteristics. However, a significant increase in the impact toughness occurs only at tempering temperatures $\geq 780^\circ\text{C}$. It is concluded that the relatively high tempering temperature required to ensure a satisfactory impact toughness is explainable by enhanced precipitation of particles of a M23C6-type carbide and (Nb, Ta)(C, N) carbonitride, which retards the retrogression processes in the lath martensite structure.

Key words: martensite, retained austenite, carbides, mechanical properties, fractography.

INTRODUCTION

Elevation of the creep resistance of high-chromium martensitic steels used for making high-pressure and ultra-high-pressure boiler tubes is an important task of the science of materials, because its solution will make it possible to raise the steam temperature in the power units of cogeneration plants, to elevate their efficiency and to reduce harmful emissions into the atmosphere. It has been shown that alloying of such steels with the aim to raise the stability of the fine particles of carbides and carbonitrides makes it possible to improve considerably their long-term creep resistance [1 – 3]. A low content of boron produces a favorable effect

on the stability of the martensitic structure under the conditions of creep due to the higher fineness and coagulation resistance of the particles of $M_{23}(\text{C}, \text{B})_6$ [4, 5]. In addition, alloying of high-chromium steels with tantalum stimulates precipitation of nanosize particles of (Nb, Ta)(C, N) carbonitride, which have a high resistance to coagulation [6]. Such particles precipitate in steels during tempering and improve not only the heat resistance but the impact toughness too. The mode for the heat treatment is chosen with allowance for the fracture toughness under dynamic loading in order to lower the susceptibility of the structure components to brittle fracture in assembly and operation.

It has been reported that the steels with elevated boron content tempered at a relatively high temperature ($700 - 750^\circ\text{C}$) have a low impact toughness [7, 8]. It is assumed that the most probable cause of this effect is the formation of carbide chains over high-angle boundaries, which

¹ Belgorod State National Research University, Belgorod, Russia (e-mail: tkachev_e@bsu.edu.ru).

² Russian State Agrarian University – Moscow Agricultural Academy n.a. K. A. Timiryazev, Moscow, Russia.

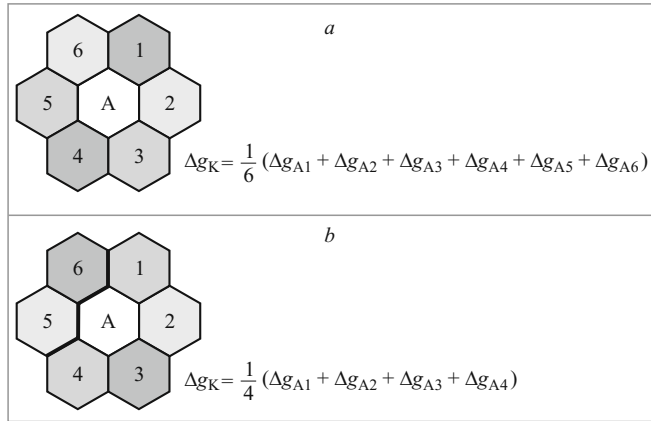


Fig. 1. Schemes and formulas for computing the average misorientation within individual grains according to Kernel: *a*, *b*) for point *A* surrounded by points with misorientations below or above the threshold value, respectively.

promotes nucleation of brittle cracks [7, 9, 10]. Segregation of boron on the high-angle boundaries of the original austenite grains can also cause embrittlement accompanied by fracture by the intergrain mechanism [11]. Another phenomenon in the temperature range mentioned is precipitation of MX-type carbides inside the martensite laths. This retards the retrogression processes and may be one more cause of reduced impact toughness.

An important phenomenon from the standpoint of practice is the temper brittleness in the temperature range of 450–550°C [7, 12]. The fracture surface of samples of martensitic steels after tempering at these temperatures consists of numerous cleavage facets with rare detachment ridges at their intersections, which is a sign of brittle transcrystalline fracture [13]. The temper brittleness is responsible for extremely low values of the impact toughness (about 5 J/cm²) even when the fracture occurs at room temperature. The lowering of the impact toughness correlates with the precipitation hardening and is often explained by precipitation of carbides of different morphologies in decomposition of retained austenite. The retained austenite in these steels has a film form and occurs chiefly on the boundaries of martensite laths and blocks. Double-stage tempering reduces the susceptibility to brittle fracture and makes it possible to keep a high strength due to variation of the sizes and distribution of carbide particles precipitated from the retained austenite [14, 15]. Thus, the spheroidization of carbides and redistribution of dislocations inside the martensite laths affect the impact toughness positively. However, there are no reported data on the relation between the microstructure and the temper brittleness of martensitic thermal engineering steels modified with boron. The changes in the microstructure under tempering and their contribution into the variation of the strength and impact toughness in these steels have not been studied exhaustively.

The aim of the present paper was to study the microstructure, the mechanical properties and the fracture mechanism of steel 10Kh9K3B2MFBR with 0.085 wt.% Ta and 0.013 wt.% B after air quenching and tempering at 200–800°C.

METHODS OF STUDY

We studied high-chromium martensitic steel with the following chemical composition (in wt.%): 0.10 C, 8.92 Cr, 3.01 Co, 1.80 W, 0.59 Mo, 0.34 Mn, 0.20 V, 0.06 Nb, 0.085 Ta, 0.03 Si, 0.013 B, 0.007 N, the remainder Fe.

An ingot with a mass of 50 kg was obtained by vacuum induction melting. The ingot was subjected to a homogenizing annealing at 1200°C for 24 h, forging at this temperature, and air cooling. The billet obtained was cut into samples with a size of 13 × 40 × 60 mm. The samples were quenched for martensite by 30-min austenitization at 1050°C and air cooling. The finishing heat treatment was tempering at 200–800°C for 3 h. After the heat treatment, we fabricated specimens for studying the microstructure and tensile and impact testing.

The laps for the scanning and transmission electron microscopy were prepared by the method of electropolishing in a 10% solution of HClO₄ in CH₃COOH at a voltage of 21 V. To obtain the EBSD patterns and to study the fracture surfaces, we used a FEI Quanta 600 FEG scanning electron microscope with a EDAX Velocity™ attachment. To assess the level of the internal microstresses, we analyzed local misorientations within individual grains by the method of Kernel [16]. We measured the average misorientation with respect to the neighbor points (Δg_K) for every point with confidence index above 0.1. The points with misorientations exceeding the threshold value (4°) were neglected as it is shown in Fig. 1*b*.

The fine structure of the steel and the particles of the second phases were studied using a JEOL JEM-2100 transmission electron microscope (TEM). The sizes of the components of the martensitic structure were determined by the method of reconstruction of the initial austenitic structure described in [17].

The tensile tests were conducted at room temperature for flat samples with the length of the test portion 25 mm and cross section 3.0 × 1.5 mm using an Instron 5882 device at deformation speed 1 mm/min. The hardness of the samples was measured after polishing their surface by the Brinell method using a Wolpert 3000BLD hardness tester at a load of 750 N and diameter of the steel ball 5 mm. We calculated the average hardness value for the results of at least five measurements. The impact toughness was determined for standard V-notched samples with cross section of the test portion 10 × 8 mm and length 55 mm using an Instron IMP 460 pendulum hammer. The volume fraction of the retained austenite was measured by the method of magnetic saturation using a FERITSCOPE FMP30 device.

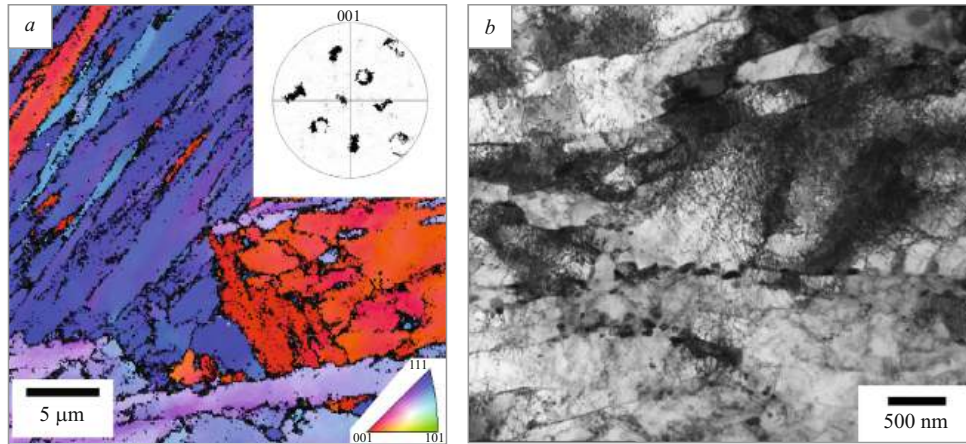


Fig. 2. Microstructure of lath martensite in Ta- and B-added steel 10Kh9K3V2MFBR after air quenching as reconstructed by EBSD analysis (*a*) and pole figure of the family of plane $\{001\}$ from the scanning range presented (*b*).

RESULTS

Structure after air quenching. Austenitization of the steel at 1050°C with subsequent air cooling produces a structure of lath martensite represented by thin martensite laths. The laths form blocks and packs surrounded by the boundaries inherited from the initial austenite grains (IAG) (Fig. 2).

The pole figure obtained by analyzing the misorientations in the EBSD map reflects the presence of a Kurdjumov–Sachs orientation relationship between the formed martensite and the initial austenite, i.e.,

$$\{111\}_{\gamma} \parallel \{011\}_{\alpha}; \quad \langle \bar{1}01 \rangle_{\gamma} \parallel \langle \bar{1} \bar{1}1 \rangle_{\alpha}. \quad (1)$$

Each of the four possible equivalent planes of the initial austenite $\{111\}_{\gamma}$ for the given orientation relationship corre-

sponds to a pack variant, and the six equivalent directions $\langle 111 \rangle_{\gamma}$ are responsible for the presence of 24 differing variants of orientation of martensite blocks in every individual IAG [18]. The average size of the IAG and of the martensite packs amounts to $46 \pm 4 \mu\text{m}$ and $2 \pm 3 \mu\text{m}$, respectively.

At 1050°C, the austenite is in equilibrium only with the particles of the (Nb, Ta)(C, N) carbonitride, the volume fraction of which is 0.09% [6] preserved in the structure of the steel after the air cooling (Fig. 3*a*). The particles have a spherical shape, and their average size after the austenitization is 38 nm. Air cooling also gives rise to precipitation of cementite particles with a lamellar morphology inside martensite laths (Fig. 3*b*). In this condition, the volume fraction of retained austenite is relatively high and amounts to $4.85 \pm 0.99\%$. The TEM study has shown the presence of

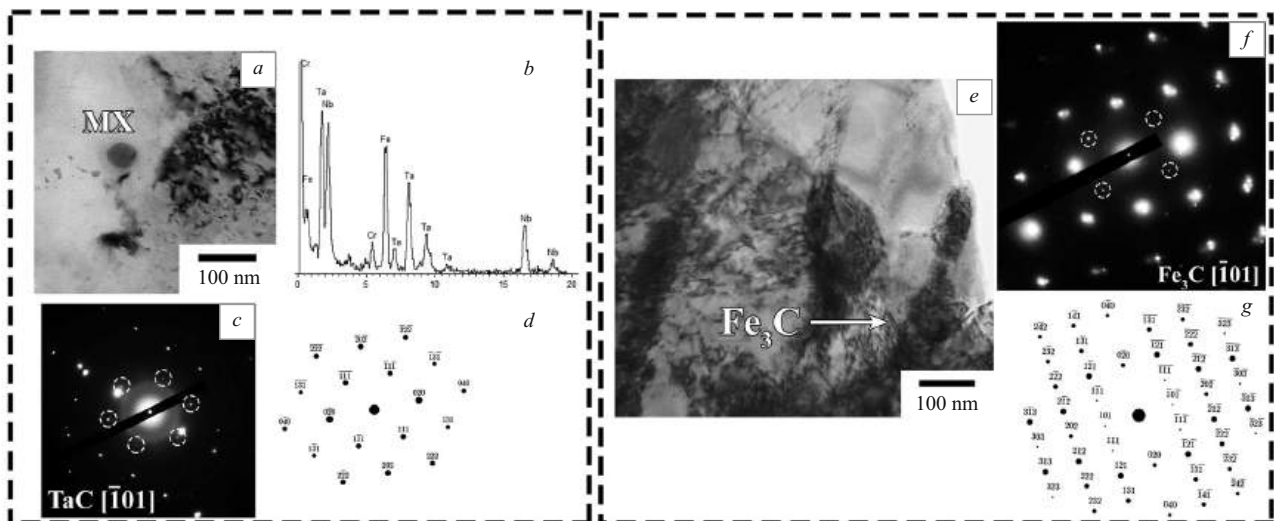


Fig. 3. Results of a complex study of the structure of particles in Ta- and B-added steel 10Kh9K3V2MFBR after air quenching (TEM): *a*–*d*) carbonitride of type MX; *e*–*g*) cementite particle inside martensite lath; *a*, *e*) against light background; *b*) curve obtained by energy dispersive chemical analysis; *c*, *f*) diffraction; *d*, *g*) simulated electron diffraction patterns.

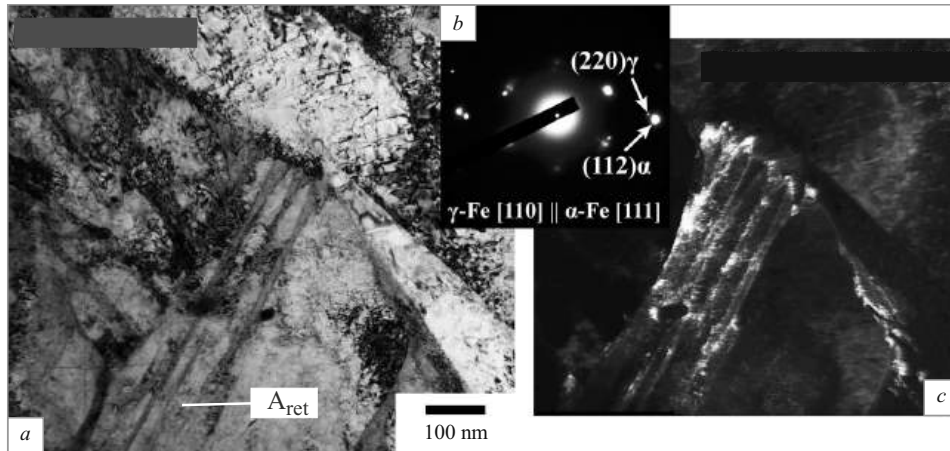


Fig. 4. Retained film-like austenite (A_{ret}) in the structure of Ta- and B-added steel after air quenching (TEM): *a*) against light background; *b*) diffraction; *c*) against dark background (γ -Fe).

film-like retained austenite inside the IAG along martensite blocks (Fig. 4).

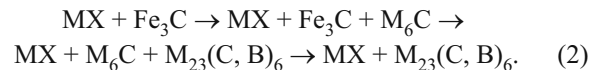
The width of the detected layers of austenite is 20–60 nm; their length exceeds 1 μm . The accommodation deformation under the martensitic transformation elevates the dislocation density inside the laths, which is well observable in Figs. 3 and 4. We have established in our previous works that the density of lattice dislocations in the air-quenched steel is about $1 \times 10^{15} \text{ cm}^{-2}$ [6, 19].

Effect of tempering on the structure and internal stresses. Figure 5*a* presents the dependence of the volume fraction of retained austenite on the tempering temperature.

When the tempering temperature is increased to 450°C, the fraction of retained austenite decreases gradually to 3%. Increase of the tempering temperature to 600°C causes total dissolution of retained austenite. The effect of the tempering temperature on the phase composition, the size of the particles and their chemical composition in the steel studied has been investigated earlier in [6]. It should be noted that cementite particles are detectable in the structure of the steel after the tempering at up to 500°C.

A considerable content of cementite particles observed in the structure is located over the boundaries of martensite laths. This allows us to think that they have formed during the dissolution of retained austenite, in contrast to the cementite particles precipitated in the process of self-tempering, and are distributed uniformly inside the laths. In addition to cementite, the steel tempered at 500°C acquires relatively coarse particles of carbide M_6C enriched with W and Mo (Fig. 6*b*). Precipitation of globular particles of carbide $M_{23}(C, B)_6$ is observable in the steel during tempering at 700–780°C. The volume fraction of these particles is the highest of all the second-phase particles, and they precipitate primarily over the intercrystalline boundaries of martensite packs, blocks and laths [6]. The $M_{23}(C, B)_6$ special carbide substitutes completely the less steady cementite at the tempering temperatures mentioned. Thus, the phase composition

evolves with increase of the tempering temperature as follows:



where MX is the (Nb, Ta)(C, N) carbonitride.

The manifested deformation contrast observed on the thin foil of the steel after tempering at 500°C indicates preservation of high internal stresses (Fig. 6*a* and *b*). To assess the evolution of the internal stresses with increase of the tempering temperature, we analyzed the EBSD maps of the orientations. Figure 7 presents the maps of the distribution of the average misorientation for neighbor points turned by an angle of 0–4° relative to each other. The linear gradient of reliability of the indexing is imposed onto the maps as a second layer. The dark regions with low reliability in Fig. 7 exhibit high-angle boundaries on which machine deciphering of the Kikuchi lines is complicated due to their superimposition. It can be seen that the regions with high average misorientation are distributed primarily near the high-angle boundaries of martensite blocks. Tempering at 500°C does not affect substantially the value of the average misorientation and the distribution of the internal microstresses in the structure. However, 2–3- μm regions with a relatively low level of microstresses are observable inside large martensite blocks. Increase of the tempering temperature to 750°C results in obvious relaxation of the microstresses in these regions and redistribution of the dislocations inside laths. The microstresses in the steel tempered at 750°C are distributed nonuniformly, but their general level remains high enough (Fig. 7*b*). The substantial decrease in the general level of microstresses after the tempering at 765 and 780°C indicates intensification of the retrogression processes. The quantitative distribution of points with respect to the misorientation angles preserves a lognormal form (Fig. 7*c*).

Effect of tempering temperature on mechanical properties. Variation of the characteristics of strength and ductility in the process of tempering is presented in Fig. 5b.

After the austenitization at 1050°C with air cooling the steel exhibited the following mechanical properties: yield strength $\sigma_{0.2} = 1020$ MPa, ultimate strength $\sigma_r = 1270$ MPa, elongation $\delta = 10.1\%$. High strength properties after air quenching are typical for heat technology steels with 9–12 wt.% chromium [2, 7, 15, 19]. Tempering at 500°C promotes elevation of the strength characteristics and inconsiderable increase in the elongation (Fig. 5b). The difference between the ultimate strength and the yield strength of the steel after air quenching is reduced substantially after tempering at 750–780°C. For example, the tempering at 780°C yields $\sigma_{0.2} = 520$ MPa, $\sigma_r = 760$ MPa, $\delta = 15.5\%$. We can see a good correlation between the dependences of the hardness and strength characteristics on the tempering temperature (Fig. 5b and c).

The hardness of the steel increases in the range of the temperatures of temper brittleness and amounts to 416 ± 9 HB at $T_{\text{temp}} = 500^\circ\text{C}$. Increase of the tempering temperature from 500 to 790°C causes continuous reduction of the hardness to 182 ± 1 HB. The impact toughness after the austenitization and air cooling is quite high for a martensitic structure and amounts to $KCV = 24$ J/cm² (Fig. 5c). Tempering at 300–500°C is accompanied by lowering of the impact toughness by more than a factor of 2. Manifested embrittlement of the steel is observed after tempering at 500°C ($KCV < 5$ J/cm²). Abrupt growth of the impact toughness by more than a factor of 5 (from $KCV = 25$ J/cm² to $KCV = 135$ J/cm²) occurs when the tempering temperature is increased from 765 to 780°C. Figure 8 presents fractures (SEM) of the samples tested for impact toughness.

We established that the steel tempered at 500°C fractured by the mechanism of brittle transcrystalline cleavage with facet size about 5 μm yielding numerous secondary cracks. Brittle fracture typical for transcrystalline cleavage was also observed in the central part of the sample tempered at 780°C despite the relatively high value of the impact toughness. At the same time, a ductile dimple fracture has been detected at the periphery of the surface (Fig. 8e). The substantial plastic deformation during the fracture in this condition caused changes in the shape of the sample (Fig. 8b).

DISCUSSION

Decrease in the average misorientation with growth of the tempering temperature correlates with the growth of the width of the martensite laths (Fig. 7b). The low-angle boundaries of the laths have a misorientation ranging within 1–3° and are hardly distinguishable in the EBSD pictures. However, the contribution of the lath boundaries into the general level of the microstresses is quite high. This is connected with the fact that they are dislocation configurations chiefly formed by same-sign dislocations, and the average

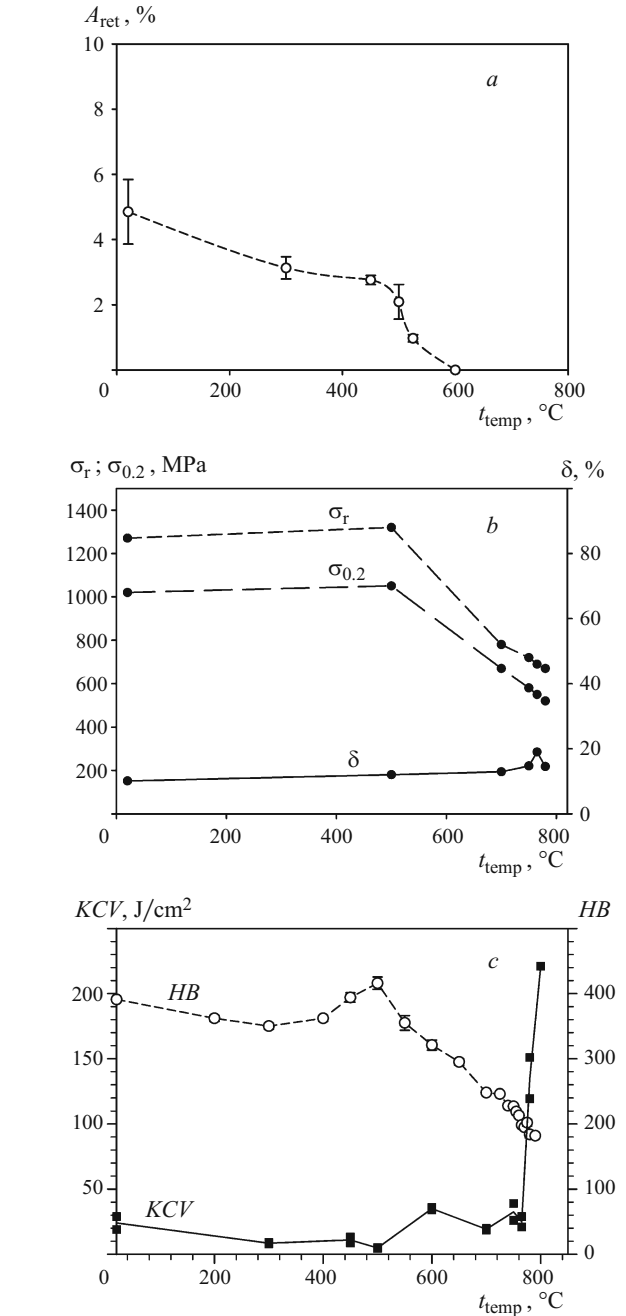


Fig. 5. Content of retained austenite (A_{ret}) in the structure (a), yield strength ($\sigma_{0.2}$), ultimate strength (σ_r) and elongation (δ) (b), hardness (HB) and impact toughness (KCV) (c) as a function of tempering temperature (t_{temp}) for Ta- and B-added steel 10Kh9K3V2MFBR.

distance between them after the air quenching amounts to about 0.2 μm (see Table 1).

The scanning step for obtaining EBSD pictures (0.15 μm) is comparable to the width of the laths. The data on the average misorientation of points on the surface of the crystal (θ_{CAM}) allowed us to calculate the tensor dislocation density by the following equation [16]:

$$\rho_{\text{KAM}} = 2\theta_{\text{KAM}}/(bh), \quad (3)$$

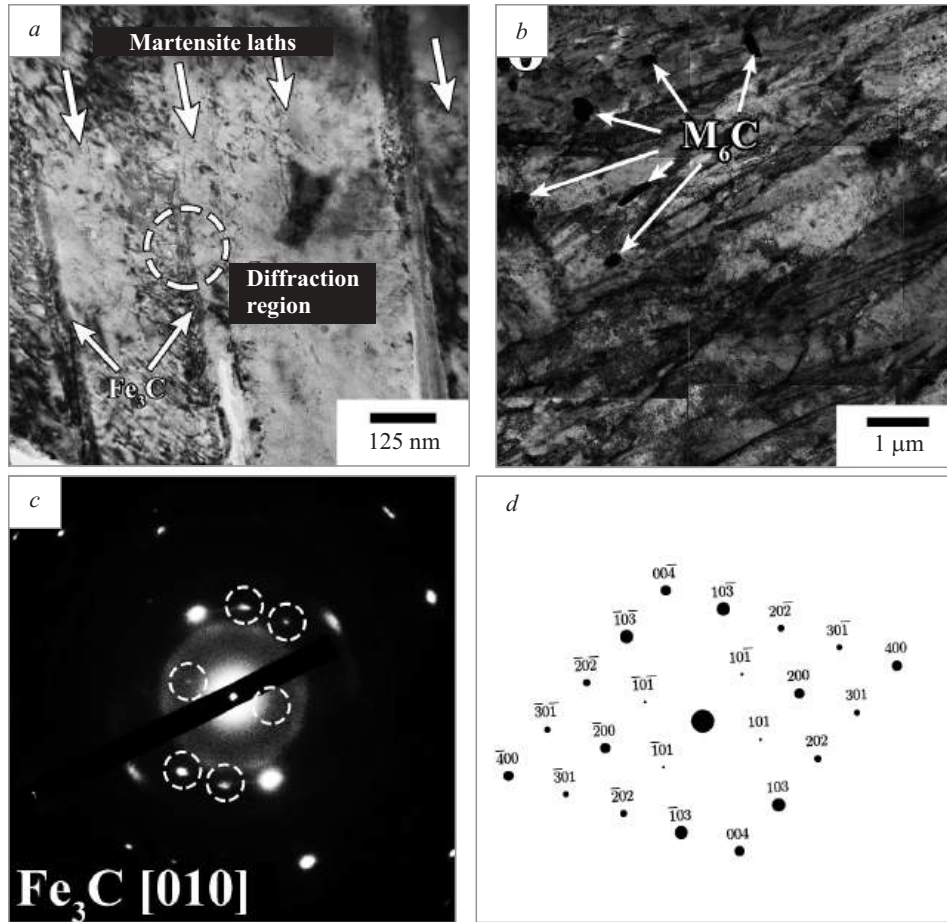


Fig. 6. Cementite layers over boundaries of martensite laths (*a*, *c*, *d*) and globular particles of M_6C carbide in the structure of Ta- and B-added steel 10Kh9K3V2MFBR after 3-h tempering at 500°C (TEM): *a*, *b*) against light background; *c*) diffraction from cementite in the encircled region; *d*) results of simulation of diffraction, axis of zone [010].

where b is the amplitude of the Burgers vector and h is the scanning step. The calculated tensor dislocation density θ_{CAM} in the steel after austenitization and air cooling

TABLE 1. Characteristics of the Lath Structure of the Steel after Tempering at Different Temperatures

$T_{temp}, ^\circ C$	$h_1, \mu m$	$\rho_{ld}, \times 10^{14} m^{-2}$	θ_{CAM}, deg	$\rho_{CAM}, \times 10^{14} m^{-2}$	$h_{HAB}, \mu m$
Initial	0.19 ± 0.02	10.04 ± 4.31	0.789	7.40	3.38
500	0.21 ± 0.02	3.48 ± 1.25	0.786	7.38	3.21
750	0.27 ± 0.02	2.31 ± 0.88	0.743	6.97	2.96
765	0.30 ± 0.03	1.20 ± 0.40	0.653	6.13	3.07
780	0.36 ± 0.04	1.67 ± 0.59	0.603	5.66	3.82

Notations: Initial — initial condition after 30-min air quenching at 1050°C; h_1) lath width; ρ_{ld}) density of lattice dislocations; θ_{CAM}) average misorientation inside grains by the method of CAM; ρ_{CAM}) tensor dislocation density; h_{HAB}) average distance between HAB (EBSD).

amounted to $7.4 \times 10^{14} m^{-2}$ (see Table 1). The obtained values of θ_{CAM} are somewhat lower than the density of the lath dislocations calculated from the results of the experimental assessment of the number of individual dislocations per unit area of the surface of thin foils with the use of TEM [6]. It seems that the tensor dislocation density receives contribution only from the uncompensated dislocations that cause turning of neighbor parts of the crystal. The close values of θ_{CAM} in the steel after the austenitization with air cooling and after tempering at 500°C indicate that the high elastic stresses and the dislocation density are preserved, and tempering at this temperature can be classified as a low-temperature one. Thus, the most probable reason behind the appearance of temper brittleness at 500°C is the additional precipitation of cementite particles over the boundaries of martensite laths due to decomposition of retained austenite and precipitation of coarse particles of a M_6C carbide. Enhancement of the degree of decomposition of retained austenite, which is a softer and less strong phase than martensite, also results in lowering of the impact toughness and

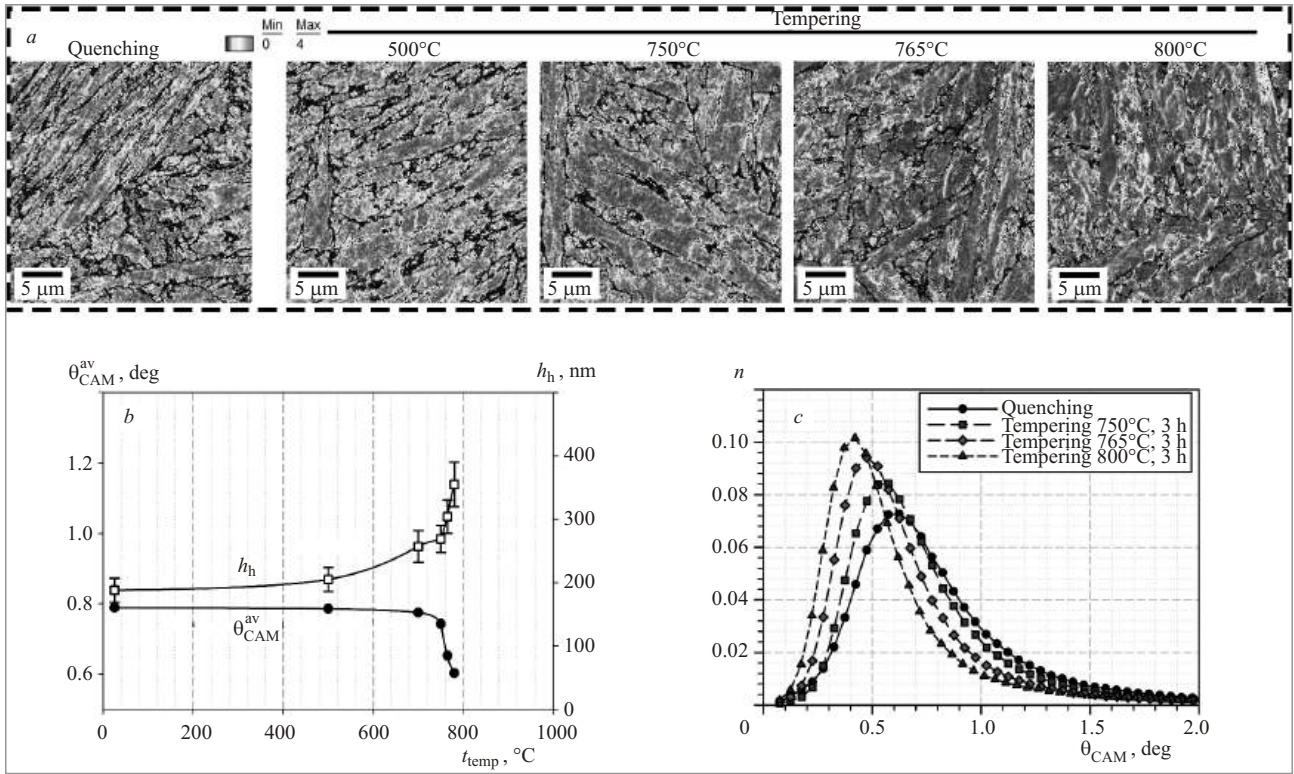


Fig. 7. Maps of distribution of the average misorientation after air quenching from 1050°C (30 min) and tempering at different temperatures (a), dependences of the average misorientation inside grains (θ_{CAM}^{av}) and of the width of martensite laths (h_h) on the tempering temperature (b), and quantitative distribution of misorientations (θ_{CAM}) after different treatment modes (c).

elevation of the strength characteristics. It is known that the distance between HAB corresponds approximately to the width of the martensite blocks, while a brittle crack propa-

gates in martensitic steels by separation over the planes of family {001} [13, 19, 20]. The comparable sizes of the brittle cleavage facets on the fracture surface and the distance be-

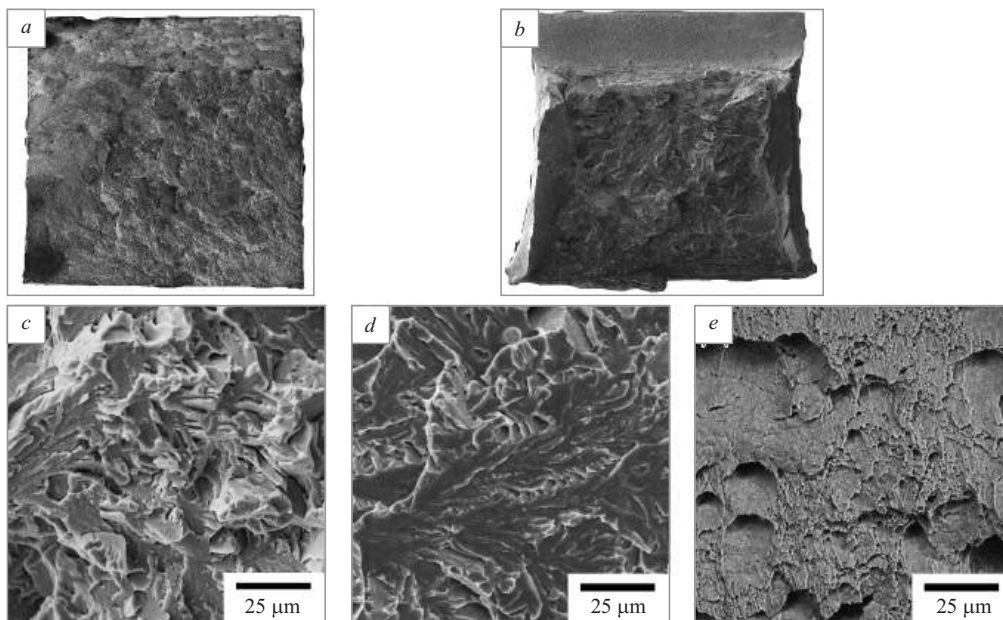


Fig. 8. Macro- (a, b) and micro-fractures (c – e) of samples tested for impact toughness: a, c) after tempering at 500°C; b, d, e) after tempering at 780°C; c, d) in the central region; e) in the region of shear lips.

tween the HAB allow us to think that the observed fractographic relief has been formed due to frequent changes in the direction of the brittle crack upon intersection with the high-angle boundaries of martensite blocks.

The lowering of the average misorientation inside grains at tempering temperatures $\geq 750^\circ\text{C}$ is a consequence of the development of the processes of migration and merging of lath boundaries and partial annihilation of dislocations inside laths. We have mentioned that alloying with boron makes the particles of $M_{23}(\text{C}, \text{B})_6$ finer. The high density of the particles of second phases in the structure hinders the retrogression processes in tempering of boron-added martensitic steels. As a consequence, the relaxation of internal stresses in these steels requires a higher tempering temperature. The impact toughness increases when the temperature is below the recrystallization threshold, because the mean distance between the HAB does not change substantially at the tempering temperatures studied (see Table 1). This allows us to infer that the transition to a ductile fracture mechanism upon increase of the tempering temperature to 780°C is explainable by decrease in the internal stresses and enhancement of the mobility of dislocations inside the martensite laths.

CONCLUSIONS

The results of the study of the microstructure, mechanical properties and fracture surfaces after impact tests of steel 10Kh9K3B2MFBR with 0.085 wt.% Ta and 0.013 wt.% B after air quenching and tempering at $300 - 800^\circ\text{C}$ allow us to make the following conclusions.

1. After the austenitization with air cooling the steel acquires a hierarchic structure of lath martensite with 4.85 ± 0.99 vol.% retained austenite with a film morphology. In this condition, the steel contains undissolved particles of (Nb, Ta)(C, N) carbonitride and cementite particles precipitated during the cooling inside the martensite laths.

2. Increase of the tempering temperature of the steel from 300 to 550°C enhances the degree of the decomposition of the retained austenite, which decomposes totally at 600°C . This process is accompanied by formation of cementite chains over the boundaries of the martensitic structure. At tempering temperatures $\geq 700^\circ\text{C}$, the special $M_{23}(\text{C}, \text{B})_6$ carbide substitutes the less stable cementite completely.

3. The accommodation deformation in the martensitic transformation causes growth of the density of lath dislocations to $1 \times 10^{15} \text{ cm}^{-2}$ and of the tensor dislocation density to $7.4 \times 10^{14} \text{ m}^{-2}$. High internal stresses are preserved in the structure of the steel after the tempering at a temperature below 750°C . The intensification of the retrogression processes upon increase of the tempering temperature from 750 to 780°C reduces the internal stresses by 20% and widens the martensite laths from 270 to 350 nm .

4. The decomposition of the retained austenite and the secondary hardening during the tempering at 500°C elevate the yield strength from 1020 to 1050 MPa and the hardness

from 391 ± 4 to $416 \pm 9 \text{ HB}$. The reduction of the impact toughness to $KCV = 5 \text{ J/cm}^2$ in such tempering is caused by formation of cementite chains over lath boundaries and of coarse $M_6\text{C}$ carbides enriched with W and Mo.

5. The elevation of the impact toughness to $KCV = 135 \text{ J/cm}^2$ and the dominance of ductile fracture on the fracture surface when the tempering temperature is increased to 780°C are connected with the lowering of the internal stresses due to intensification of retrogression processes and precipitation of globular particles of grain-boundary carbide $M_{23}(\text{C}, \text{B})_6$.

This study has been supported financially by an intra-university grant "Young Leaders in Science" of the National Research University "BelSU" in 2023. The authors thank the Joint Research Center "Technology and Materials" of the Belgorod State National Research University, which is supported financially by the Ministry of Science and Higher Education of the Russian Federation within the framework of Agreement No. 075-15-2021-690, for using the equipment.

REFERENCES

1. S. Albert, M. Kondo, M. Tabuchi, et al., "Improving the creep properties of 9Cr-3W-3Co-NbV steels and their weld joints by the addition of boron," *Metall. Mater. Trans. A*, **36**, 333-343 (2005).
2. A. Fedoseeva, I. Nikitin, N. Dudova, and R. Kaibyshev, "Analysis of mechanical properties of refractory Co-modified 12% Cr and 8% Cr steels," *Fiz. Met. Metalloved.*, **121**(12), 1338-1344 (2020).
3. E. Tkachev, A. Belyakov, and R. Kaibyshev, "Creep strength breakdown and microstructure in a 9% Cr steel with high B and low N contents," *Mater. Sci. Eng. A*, **772**, Art. 138821 (2020).
4. F. Abe, T. Horiuchi, M. Taneike, and K. Sawada, "Stabilization of martensitic microstructure in advanced 9Cr steel during creep at high temperature," *Mater. Sci. Eng. A*, **378**(1-2), 299-303 (2004).
5. E. Tkachev, A. Belyakov, and R. Kaibyshev, "Role of deformation in coagulation of particles of $M_{23}C_6$ carbide in 9% Cr steel," *Fiz. Met. Metalloved.*, **121**(8), 884-891 (2020).
6. E. Tkachev and R. Kaibyshev, "Effect of tempering on the precipitation behavior of a Ta-alloyed 9% Cr steel with high B and low N contents," *Mater. Today Commun.*, **32**, 103938 (2022).
7. R. Mishnev, N. Dudova, V. Dudko, and R. Kaibyshev, "Impact toughness of a 10% Cr steel with high boron and low nitrogen contents," *Mater. Sci. Eng. A*, **730**, 1-9 (2018).
8. R. Klueh, D. Alexander, and M. Sokolov, "Effect of chromium, tungsten, tantalum, and boron on mechanical properties of 5-9Cr-WVTaB steels," *J. Nucl. Mater.*, **304**(2-3), 139-152 (2002).
9. R. Mishnev, N. Dudova, R. Kaibyshev, and A. Belyakov, "On the fracture behavior of a creep resistant 10% Cr steel with high boron and low nitrogen contents at low temperatures," *Materials*, **13**(1), Art. 3 (2019).
10. S. Kotrechko, Yu. Meshkov, and R. Televich, "Effect of the sizes of martensite packs and carbide particles on the "brittle" strength of low-carbon martensitic steels," *Metall. Term. Obrab. Met.*, No. 9, 28-34 (2006).

11. Y. Liu, S. Tsukamoto, K. Sawada, et al., "Precipitation behavior in the heat-affected zone of boron-added 9Cr – 3W – 3Co steel during post-weld heat treatment and creep deformation," *Metall. Mater. Trans. A*, **46**, 1843 – 1854 (2015).
12. I. Fedorova, A. Kostka, E. Tkachev, et al., "Tempering behavior of a low nitrogen boron-added 9% Cr steel," *Mater. Sci. Eng. A*, **662**, 443 – 455 (2016).
13. R. Vorob'ev, V. Dubinskii, and V. Evstifeeva, "Effect of self-tempering and tempering processes on mechanical characteristics and fracture behavior of air-quenched low-carbon martensitic steel," *Fiz. Met. Metalloved.*, **120**(10), 1083 – 1088 (2019).
14. A. Makovetslkii, D. Mirzaev, L. Yusupova, et al., "Mechanical properties of turbine steel after complete quenching with stabilization of austenite," *Fiz. Met. Metalloved.*, **120**(10), 1066 – 1071 (2019).
15. M. Odnobokova, A. Kipelova, A. Belyakov, and R. Kaibyshev, "Mechanical behavior and brittle-ductile transition in high-chromium martensitic steel," *Fiz. Met. Metalloved.*, **117**(4), 404 (2016).
16. M. Calcagnotto, D. Ponge, E. Demir, and D. Raabe, "Orientation gradients and geometrically necessary dislocations in ultra-fine grained dual-phase steels studied by 2D and 3D EBSD," *Mater. Sci. Eng. A*, **527**(10 – 11), 2738 – 2746 (2010).
17. F. Niessen, T. Nyysönen, A. A. Gazder, and R. Hielscher, "Parent grain reconstruction from partially or fully transformed microstructures in MTEX," *J. Appl. Crystallog.*, **55**(1), 180 – 194 (2022).
18. M. Lobanov, G. Rusakov, A. Redikultsev, et al., "Investigation of special misorientation in lath martensite of low-carbon steel by the method of orientation microscopy," *Fiz. Met. Metalloved.*, **117**(3), 266 (2016).
19. E. Tkachev, A. Belyakov, and R. Kaibyshev, "Effect of hot-rolling on the microstructure and impact toughness of an advanced 9% Cr steel," *Crystals*, **13**(3), Art. 492 (2023).
20. N. Polekhina, V. Linnik, I. Litovchenko, et al., "The microstructure, tensile and impact properties of low-activation ferritic-martensitic steel EK-181 after high-temperature thermo-mechanical treatment," *Metals*, **12**(11), Art. 1928 (2022).